ACS APPLIED MATERIALS & INTERFACES

Research Article

www.acsami.org

Porous Polystyrene-*Block*-Poly(Acrylic Acid)/Hemoglobin Membrane Formed by Dually Driven Self-Assembly and Electrochemical Application

Jiaqi Xu, Zhengxi Zhu, and Huaiguo Xue*

College of Chemistry and Chemical Engineering, Yangzhou University, Yangzhou, Jiangsu 225002, China

Supporting Information

ABSTRACT: This study demonstrated a facile method to form a porous polymeric membrane, immobilizing a biocatalyst. A polyelectrolyte-based amphiphilic diblock copolymer, i.e., polystyrene-*block*-poly(acrylic acid) (PS-*b*-PAA), self-assembled with hemoglobin (Hb) dually driven by charge and amphiphilicity during solution-casting and evaporation. XPS and contact angle measurements suggested that the PS block enriched on the membrane surface. The PAA block pointed toward the internal membrane as well as ordered the Hb arrangement at the interface of the polymer and electrode. The obtained PS-*b*-PAA/Hb electrode showed a remarkably enhanced direct electron transfer (ET), which was revealed to be a surface-controlled process accompanied by single-proton transfer. The membrane was tested to catalyze the reduction of hydrogen peroxide, and exhibited an excellent reproducibility and stability. This method with a charge and amphiphilicity dually driven (CADD) self-assembly opened up a new way to construct a third-generation electrochemical biosensor.

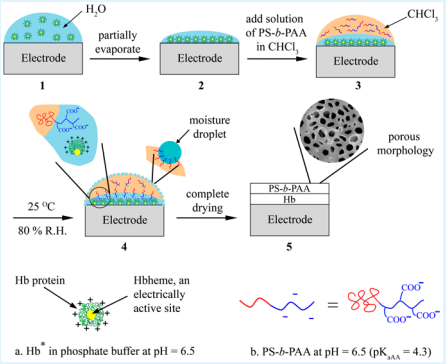

KEYWORDS: *dually driven self-assembly, porous membrane, amphiphilic diblock copolymer, electrocatalysis, direct electron transfer*

1. INTRODUCTION

A biomimetic membrane is a key component of biosensors and biofuel cells. It is crucial for a bioactive molecule to sustain its bioactivity as well as to reach a high concentration in a membrane. An ordered arrangement of biomolecules in a membrane and exposure of their electroactive centers are also desirable for a high sensitivity. To achieve this goal, researchers have devoted great efforts to construction design, material selection, and technique creation.[1−5] Conventional methods for immobilizing a catalytic biomolecule on electrode surface include adsorption,[6] cross-linking of biomolecules,[7] covalent bonding,[8,9] embedment,[10−12] electrochemical polymerization,[13] and self-assembly.[5,14−16] Various supporting materials, e.g., $CaCO_3$ nanoparticles,[17] conducting polymers,[18] hydrogels,[19] and clays,[20] have been successfully utilized to anchor biomolecules. Among them, polymers have been more attractive because of their relatively better film-forming ability, biocompatibility, and adhesion to a substrate, which helps an electrode obtain reproducible and stable performances.[13,18,19,21−23] However, it is still very difficult to fabricate a polymeric membrane, where biomolecules are able to be orderly arranged so as to facilitate a direct electron transfer (ET) from the biomolecule to an underlying substrate.

A porous membrane with a large surface area could provide a high permeability to a reactant and is expected to be a promising candidate for a biocatalyst carrier. Maruyama et al.[24] and Yabu et al.[25] found that a porous polymeric film can be fabricated by casting a solution of an amphiphilic polymer in a volatile and water-immiscible solvent under a humid atmosphere. The volatile solvent evaporated rapidly and the surface temperature dramatically decreased. Water vapor in the humid atmosphere condensed onto the surface of the water-immiscible solution and formed water droplets with a diameter of several micrometers. The amphiphilic polymer as a surface active agent prevented the water droplets from coalescence. After the evaporation of the solvent, the temperature rose back to the room temperature. The water droplets subsequently evaporated, leaving porous surface.[24,26−29] A porous electrode membrane can be formed.

In this study, a polyelectrolyte-based amphiphilic diblock copolymer (i.e., PS-*b*-PAA) was used to form a porous membrane, immobilizing a catalytic biomolecule (i.e., hemoglobin (Hb)). PS-*b*-PAA orderly assembled at the oil/water interface driven by its amphiphilicity. Since the PAA block was negatively charged and the biomolecule positively charged at specific pH, the organized PS-*b*-PAA was able to assemble the biomolecule by a charge−charge interaction. This study used a positively charged Hb as a model biomolecule, which was an iron-containing oxygen-transport metalloprotein in red blood cells.[30] It was an ideal model to study electron transfer (ET) between a protein and electrode substrate because of its commercial availability, moderate cost and a well-documented

Received: February 14, 2015
Accepted: April 6, 2015
Published: April 6, 2015

DOI: 10.1021/acsami.5b01487
ACS Appl. Mater. Interfaces 2015, 7, 8852−8858

structure. However, facilitation of this ET was considered to be very challenging, because Hb had an extended three-dimensional structure and inaccessibility of the electroactive center. With this charge and amphiphilicity dually driven (CADD) self-assembly, this study showed that PS-*b*-PAA and Hb had good synergism on the electrochemical activity of Hb, and the direct ET was remarkably enhanced. The electrode was tested to rapidly and conveniently determine hydrogen peroxide. This facile technique opened up a way to construct a third-generation electrochemical biosensor.

2. EXPERIMENTAL SECTION

2.1. Materials. An Hb molecule has a dimension of 5.3 × 5.4 × 6.5 nm^3 and a molecular weight of ~64500 g mol^{-1}. The molecule typically has four subunits in roughly a tetrahedral arrangement. Each subunit is a globular protein embedding Hbheme, an electroactive center. Each Hbheme consists of an iron ion held in a heterocyclic ring, known as a porphyrin. This porphyrin ring consists of four pyrrole molecules cyclically linked together by methine bridges, and is capable to coordinate with an iron ion within the ring. Bovine Hb was purchased from Fluka with 64.5 kDa and ~95% (protein basis). PS-*b*-PAA (Product ID, P4873A-SAA; $\bar{M}_n$, PS (16000 g mol^{-1}) and PAA(4300 g mol^{-1}); $\bar{M}_w/\bar{M}_n$ = 1.5), was purchased from the Polymer Source, Inc. (as shown in Scheme 1). All other chemicals used were of

Scheme 1. Chemical structure of PS-*b*-PAA ($\bar{m}$ = 154 and $\bar{n}$ = 60)

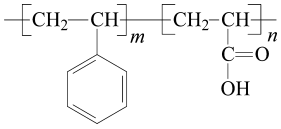

analytical grade and used as received. $CHCl_3$, Na_2HPO_4, and NaH_2PO_4 were purchased from the Shanghai Reagent Company. pH of the phosphate buffer (PB) solution was adjusted to 6.5 with 0.1 M of Na_2HPO_4 and NaH_2PO_4 in total, at which acrylic acid units were negatively charged (pK_a = 4.3), whereas an Hb was in positive (pI = 6.8). KBr and H_2O_2 were purchased from the Sinopharm Chemical Reagent Co., Ltd. All aqueous solutions were prepared with deionized water. H_2O_2 was freshly diluted before usage.

2.2. Apparatus. An electrochemical workstation (model CHI660A by the CH Instruments) was used for cyclic voltammetric (typically the third cycle was used for data analysis to obtain a stead-state CV cycle) and amperometric measurements. A three-electrode cell system included a saturated calomel electrode (SCE) as a reference electrode, a platinum sheet as a counter electrode (5 × 6 mm^2), and a modified glassy carbon electrode (GCE) (3 mm in diameter) as a working electrode on which PS-*b*-PAA/Hb film formed. The cell was 23 mm in inner diameter, and 54 mm in height. Electrolyte solutions in the cell (typically 10 mL) were purged with highly purified nitrogen for at least 20 min prior to the series of experiments, and were kept under nitrogen atmosphere during the rest of the measurements. Fourier transform infrared (FTIR) spectra were recorded by a Tensor 27 spectrometer, PS-*b*-PAA/Hb was formed on a metal sheet as it prepared on an electrode. After being dried in the chamber, the film was peeled off and further dried under an infrared lamp. A small piece of the film was grinded and tableted with KBr powder for an FTIR measurement. The sample film was also coated with a 40 Å layer of Au by a Bal-Tel SCD 500 sputter, and then was imaged with a XL-30E scanning electron microscope (SEM) (Philips, Netherland). Adjustable micropipettes (model Z 37146, ZX 13939, and KZ 14360 from the Shanghai Thermo Electron Corporation) were used for solution preparation and transfer. An ultrasound machine (Model KQ–300VDE, the KunShan Ultrasound Instruments) was used for cleaning the working electrode. A temperature and humidity controlled chamber (the Shanghai Shengli company) was used for storing and drying the samples. A 3D stylus surface profilometer (Nanomap-500LS, the AEP Technology) was used to measure a membrane thickness.

2.3. Electrode Preparation. A GCE with a diameter of 3 mm was polished by abrasive cloth with a layer of 0.5 and 0.05 μm of alumina grains sequentially, and then was cleaned by ultrasound in ethanol and deionized water respectively for 2–3 min each. The GCE was rinsed with deionized water, and dried by air blowing. PS-*b*-PAA was dissolved in $CHCl_3$, and Hb in 0.1 M of PB solution at pH 6.5. To obtain CV with a higher response to PS-*b*-PAA/Hb, we optimized the concentration and the mass ratio of Hb over PS-*b*-PAA by running a series of experiments, and then the optimal concentrations of Hb and PS-*b*-PAA were chosen in this study. In a typical sample preparation, 6 μL of Hb (1 mg mL^{-1}) was spread evenly onto the surface of the GCE (see Figure 1). The coated electrode was put in the air at room

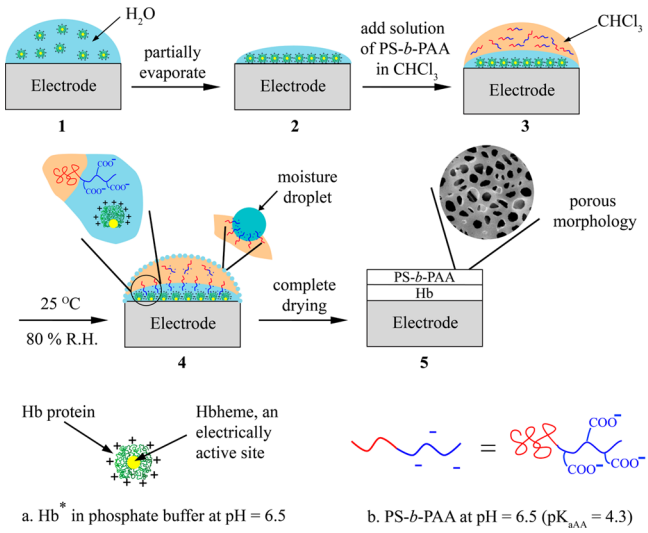

Figure 1. Scheme of the PS-*b*-PAA/Hb membrane formation on the electrode; *Hb is demonstrated as one of its four subunits.

temperature for about 20 min. The most of water was evaporated, and the sample was partially dried. 7 μL of PS-*b*-PAA (0.05 wt %) was then cast on the top of the Hb layer. The sample was put into a temperature and humidity controlled chamber (25 °C and 80% R.H.) for drying.

As controls, typically two electrodes were prepared. A PS-*b*-PAA electrode was prepared by spreading 7 μL of PS-*b*-PAA (0.05 wt %) $CHCl_3$ solution onto the GCE, and then dried in a temperature and humidity controlled chamber (25 °C and 80% R.H.). An Hb electrode was prepared by spreading 6 μL of Hb (1 mg mL^{-1}) onto the surface of the GCE and then drying it in the open air. Since the Hb layer without a polymer was easy to be washed off after a couple of electrical measurements, either a bare GCE or above PS-*b*-PAA electrode in an Hb (1 mg mL^{-1}) PB solution was also directly used for a CV measurement. Besides those controls, for a contact angle measurement, an extra PS-*b*-PAA electrode was prepared by spreading 7 μL of PS-*b*-PAA (0.05 wt %) $CHCl_3$ solution onto the GCE, and dried in the open air.

3. RESULT AND DISCUSSION

3.1. Characterization of PS-*b*-PAA/Hb Film. FTIR spectrometry is an effective way to monitor the changes of Hb. In the IR spectrum in Figure 2, appearance of peaks at 698, 754, and, 1389 cm^{-1} in the spectrum of PS-*b*-PAA/Hb rather than in the ones of either PS-*b*-PAA or Hb suggested interactions (e.g., ionic bonds) between PS-*b*-PAA and Hb, which as discussed in the following paragraphs (shown in the step 4 of Figure 1) may induce the distortion of the protein

DOI: 10.1021/acsami.5b01487
ACS Appl. Mater. Interfaces 2015, 7, 8852–8858

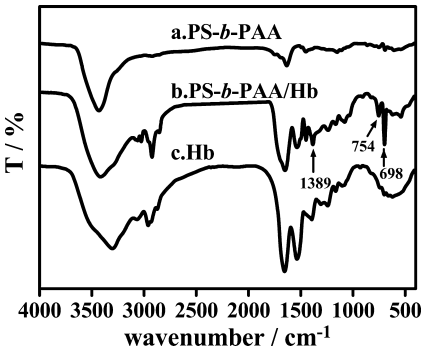

Figure 2. FTIR spectra for (a) PS-*b*-PAA, (b) PS-*b*-PAA/Hb, and (c) Hb, indicating the presence of the interactions between PS-*b*-PAA and Hb.

shell of Hb and the exposure of the Hbheme core to the electrode.

To better understand the formation of the PS-*b*-PAA membrane on the GCE, an SEM image was taken. Figure 3

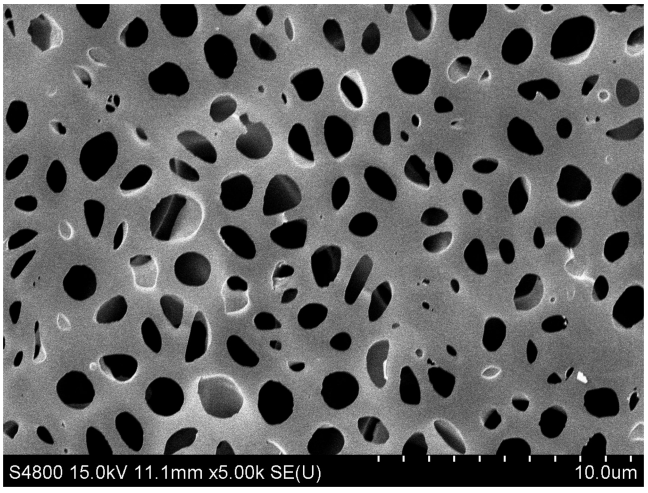

Figure 3. SEM image of the porous PS-*b*-PAA/Hb membrane.

showed that the membrane had porous surface, which was expected to have a large surface area and high permeability to reactants. The thickness measurements showed that the thickness of the nonporous membrane prepared and dried in the open air was 1.7 μm, whereas the porous one was 5.9 μm and much thicker than the nonporous one, indicating a high porosity.

The formation of the porous morphology with a polymer alone made via solvent casting and evaporation had been investigated in previous studies.[25,31,32] Therein, the amphiphilicity of the polymer drove the self-assembly at oil/water interface to form porous surface. Here we used a polyelectrolyte based amphiphilic diblock copolymer. First, an Hb water solution was cast on the electrode surface (see Figure 1). Before water entirely evaporated, the PS-*b*-PAA $CHCl_3$ solution was cast on the top of the Hb layer. $CHCl_3$ evaporated into air, dramatically decreasing the temperature of the $CHCl_3$ surface. Water vapor in the air inside the chamber condensed onto the sample surface to cover the PS-*b*-PAA layer with water droplets, the amphiphilic PS-*b*-PAA played a role of surface active agent to prevent the packed water droplets from coalescence. The negatively charged carboxyl groups of PAA electrostatically interacted with the positively charged globular Hb proteins. The organized PS-*b*-PAA was able to assemble the ordered arrangement of Hb driven by charge. The above process on the membrane formation was called as a CADD self-assembly in this study. Meanwhile, this charge−charge interaction could induce the distortion of the protein shell of Hb and the exposure of the Hbheme core to the electrode. The direct ET was expected to be enhanced.

To compare the hydrophobicity of the PS-*b*-PAA membrane with the PS-*b*-PAA/Hb one, the contact angle was measured. Either a PS-*b*-PAA/Hb or a pure PS-*b*-PAA membrane was prepared and dried in a chamber (25 °C and 80% R.H.) to form porous surface. Besides those typical controls, a pure PS-*b*-PAA membrane was prepared and dried in the open air to form nonporous surface. The result in Figure 4 showed that not

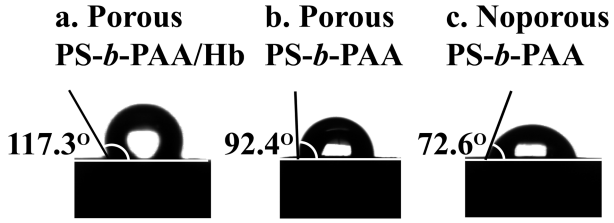

Figure 4. Water contact angle on (a) porous PS-*b*-PAA/Hb, (b) porous PS-*b*-PAA, and (c) nonporous PS-*b*-PAA membranes, suggesting that not only the porosity (b vs c) but also the surface hydrophobicity itself (a vs b) attributed to the increase of the contact angle, and that PS blocks were more on the surface of PS-*b*-PAA/Hb than PS-*b*-PAA.

only the porosity (Figure 4b vs c) but also the intrinsic surface hydrophobicity (Figure 4a vs b) attributed to the increase of the contact angle, suggesting that in the PS-*b*-PAA/Hb membrane more PS directed to the external air and PAA to the inner Hb.

To verify more PS and less PAA on the surface of PS-*b*-PAA/Hb than PS-*b*-PAA, XPS was used to measure the surface content of O and C (Figure 5). The peak of O_{1s} appears at 532 eV. The peak area of O_{1s} in Curve a was larger than that in Curve b. It was found that there was no peak of N_{1s} in the XPS trace around 400 eV, indicating no Hb appeared on the membrane surface. For a single PS-*b*-PAA chain, the content of O was 7.81%. The XPS data showed that the surface of PS-*b*-

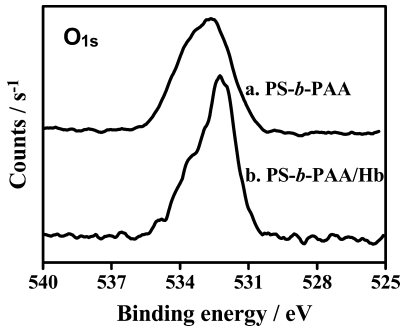

Figure 5. O_{1s} peak of the XPS samples of (a) PS-*b*-PAA and (b) PS-*b*-PAA/Hb (the peak area for each sample was normalized with O_{1s} and C_{1s}). The surface of PS-*b*-PAA alone contained 6.23% O, whereas the surface of PS-*b*-PAA/Hb contained 4.67% O. The smaller O content on the surface of PS-*b*-PAA/Hb than on PS-*b*-PAA suggested that more PAA pointed to the inner Hb and GCE substrate.

DOI: 10.1021/acsami.5b01487
ACS Appl. Mater. Interfaces 2015, 7, 8852−8858

PAA alone contained 6.23% of O, while surface of PS-*b*-PAA/Hb contained 4.67% of O. The less O on the surface of PS-*b*-PAA/Hb than PS-*b*-PAA suggested that more PAA pointed to the inner Hb and GCE substrate, which was consistent with the results from the contact angle measurements.

3.2. Direct Electrochemical Properties of PS-*b*-PAA/Hb Electrode. To characterize the direct electrochemical behaviors of the obtain electrode, the CV curves were recorded at a scan rate of 100 mV s^{-1} in a PB solution with pH 6.5. Curve a in Figure 6 showed a pair of quasi-reversible peaks for

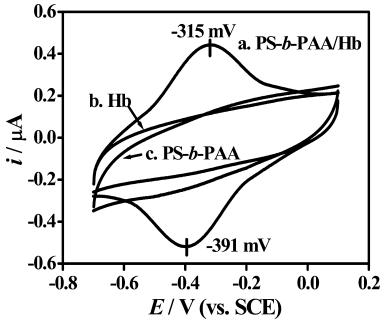

Figure 6. CV curves of (a) PS-*b*-PAA/Hb, (b) Hb, and (c) PS-*b*-PAA in 0.1 M of PB with pH 6.5 at a scan rate of 100 mV s^{-1}.

the Hb Fe(III)/Fe(II) redox couple. The anodic peak potential (E_{pa}) and cathodic peak potential (E_{pc}) were located at −315 and −391 mV, respectively. Its formal potential (E^o), defined as an average of E_{pa} and E_{pc}, was −353 mV. The peak separation, $\Delta E_p = E_{pa} - E_{pc}$, was 76 mV, which was larger than the theoretical reversible one of 58 mV[33] with the peak current ratio of $I_{pa}/I_{pc} = 1$, which indicated that the electrochemical process was quasi-reversible.[16,17,34,35] However, no redox peak was observed at either Hb or porous PS-*b*-PAA alone on the GCE substrate (Curve b and c in Figure 6). The absence of the peak in CV by Hb itself was consistent with the reports where Hb was deposited on GCE surface[36] or even in a solution.[37] Either a bare GCE or a porous PS-*b*-PAA electrode in a PB solution of Hb (1 mg·mL^{-1}) was tested by CV and no Hb peak was observed. The inertness of Hb was due to that the electroactive center, i.e., Hbheme, in its natural state was hidden inside its protein pocket. Moreover, by mixing the Hb and PS-*b*-PAA solutions and casting the mixture, no redox peak can be observed as well. These suggested that the ordered arrangement of the polymer and Hb via the CADD self-assembly was crucial for the synergism of PS-*b*-PAA with Hb to expose the electroactive center and enhance a direct ET.

Figure 7 displayed CV curves of PS-*b*-PAA/Hb with different scan rates (ν). For each curve, the peaks of the redox couple had almost an equal height. The peak current (I_p) varied linearly with the scan rate (ν) as shown in the inset A of Figure 7. This linear relation indicated a surface-controlled electrode process rather than a diffusion controlled one.[36] The slope was 0.94 by a linear regression of log I_{pc} vs log ν for Hb (inset B of Figure 7), which was close to 1.0, a characteristic value of a surface-controlled process. These two approaches were consistent to each other. The ET rate constant (k_s) could be estimated according to an equation, $k_s = mnF\nu/RT$, if the peak-to-peak separation was less than 200 mV,[38] where m was a parameter related to the peak-to-peak separation and estimated to be 0.15 s^{-1}, n was the number of transferred electrons and equal to 1, F was the Faraday constant of 96485 C mol^{-1}, R was

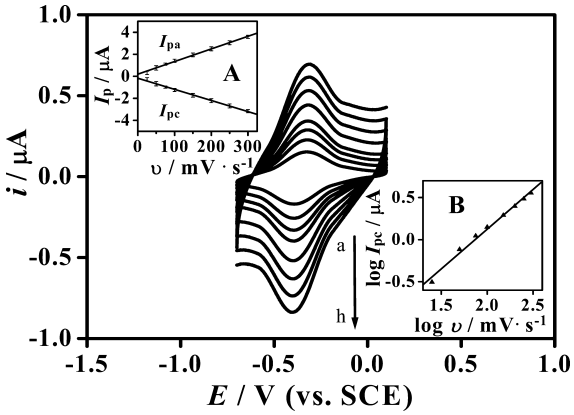

Figure 7. CVs of PS-*b*-PAA/Hb in 0.1 M PB solution with pH 6.5 and a varying scan rate. The scan rate from the inner to the outer was (a) 25, (b) 50, (c) 75, (d) 100, (e) 150, (f) 200, (g) 250, and (h) 300 mV s^{-1}, respectively. Inset A: plot of either anodic peak current (I_{pa}) or cathodic peak current (I_{pc}) vs scan rate (ν); inset B, plot of logarithm of I_{pc} vs logarithm of ν.

the universal gas constant of 8.31 J K^{-1} mol^{-1}, ν was a scan rate, and T was temperature in Kelvin. The k_s value was estimated to be 0.87 s^{-1} at a scan rate of 150 mV s^{-1}, which was similar to that of a poly(AN-*co*-AA)/Hb membrane (0.58 s^{-1}).[36] Therefore, the PS-*b*-PAA/Hb membrane formed by the dually driven self-assembly provided a favorable microenvironment for Hb and enhanced the ET.

In most of the cases, the solution pH is essential to the electrochemical behaviors of proteins. Generally, E^o of the redox couple depended on the solution pH, which indicated the participation of proton in the redox process. The CVs of PS-*b*-PAA/Hb at different pH were measured at a scan rate of 100 mV·s^{-1} (Figure 8). Clearly, the largest peak current appears

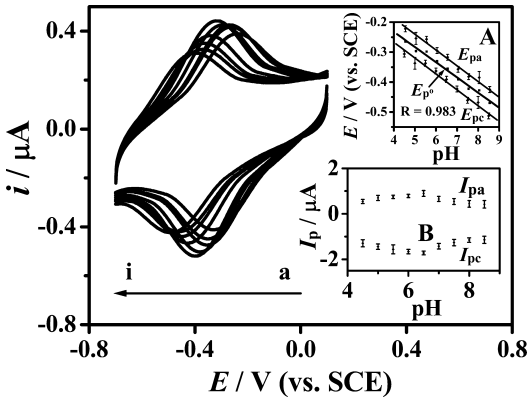

Figure 8. CVs of PS-*b*-PAA/Hb in 0.1 M of PB solution with a varying pH of (a) 4.5, (b) 5.0, (c) 5.5, (d) 6.0, (e) 6.5, (f) 7.0, (g) 7.5, (h) 8.0, and (i) 8.5, at 100 mV s^{-1}; inset A, plot of E_{pa}, $E_{p\theta}$, E_{pc} vs pH; inset B, plot of I_{pa}, I_{pc} vs pH.

between the pH of 6.0 and 7.0 (Inset B of Figure 8). This might be due to hemoglobin in these pH values got the best biological activity. An increase of the solution pH from 4.5−8.5 led to a negative shift of both oxidation and reduction peak potentials. The formal potential was found to be linearly decreased with increasing pH from 4.5 to 8.5 (a-i) with a slope of −50.7 mV·pH^{-1} (Inset A of Figure 8). This value was considered to be close to the theoretical value of −57.6 mV·pH^{-1} for a reversible proton-coupled single ET,[39] and suggested that the ET

DOI: 10.1021/acsami.5b01487
ACS Appl. Mater. Interfaces 2015, 7, 8852−8858

between the electrode and a heme group of an Hb was a process accompanied by single protonation, which can be represented in a general term as

$$\text{Hbheme[Fe(III)]} + \text{H}^+ + \text{e}^- \leftrightarrow \text{Hbheme[Fe(II)]}$$

where the charges on Hb species were not labeled.

3.3. Electrocatalysis of PS-*b*-PAA/Hb Electrode toward H_2O_2. Hb can be employed to catalyze the reduction of hydrogen peroxide because of its similarity with peroxidase. The electrocatalytic behavior of the PS-*b*-PAA/Hb electrode on H_2O_2 was observed by the CV (Figure 9). When H_2O_2 was

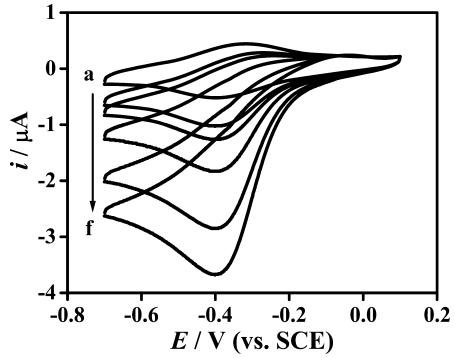

Figure 9. CVs of PS-*b*-PAA/Hb in 0.1 M of PB solution with pH 6.5: (a) no H_2O_2 and (b) 0.2, (c) 0.3, (d) 0.6, (e) 1.5, and (f) 3.0 mM H_2O_2; scan rate 100 mV s^{-1}.

added into 0.1 M of PB solution with pH 6.5, the reduction peak increased, and the oxidation peak decreased. The reduction peak current increased as the H_2O_2 concentration increased (Figure 9, curves b–f), indicating that the immobilized Hb exhibited an electrocatalytic behavior on the H_2O_2 reduction.

An amperometry method was considered to be an effective way to evaluate performances of a biosensor. The PS-*b*-PAA/Hb electrode was thus tested with H_2O_2 at a constant potential of −0.25 V (vs SCE). Figure 10 showed the response curves during successive injections of H_2O_2 into a PB solution with pH 6.5. The inset A of Figure 10 was the calibration curve of

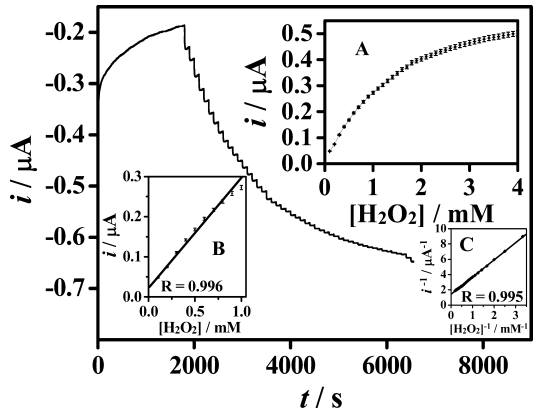

Figure 10. Typical curve of steady-state responses with a successive injection of H_2O_2 into 10 mL of 0.1 M PB solution and fast stirring (potential, −250 mV; injection interim, 100 s). Inset A, calibration curve of PS-*b*-PAA/Hb for H_2O_2; inset B, linear range of the curve in inset A from 20 to 1.0×10^3 μM; inset C, linear calibration curve of i^{-1} vs $[H_2O_2]^{-1}$, giving the Michaelis constant of 1.60 mM.

H_2O_2. The sensitivity of the electrode was determined to be 4.0 mA M^{-1} cm^{-2} by the slope of Inset B and the electrode area. The electrode achieved 95% of the steady-state current within 9 s, having a linear range from 20 to 1.0×10^3 μM. The detection limit was 12 μM based on a signal-to-noise ratio of 3. Compared with several kinds of electrodes in other studies, e.g., a carbon nanotube electrode (a linear range of 210–900 μM, and a detection limit of 9 μM) by Zhao et al.,[40] a graphene/ZnS electrode (10–250 μM, and 1.1 μM) by Wang et al.,[41] a MoS_2 electrode (20–180 μM, and 6.7 μM) by Liu et al.,[42] a triacetone triperoxide electrode (19–117 μM and 5.5 μM) by Jian et al.,[43] a chitosan/$CaCO_3$ electrode (37–830 μM, and 8.3 μM) by Shan et al.,[44] the fabricated electrode in this study showed a moderately and sufficiently wide detection range and comparable detection limit for a real application. The apparent Michaelis constant can be calculated by analyzing the slope and the intercept of a plot of reciprocals of the calibration curve (Inset C of Figure 10), and was 1.60 mM for the PS-*b*-PAA/Hb membrane obtained in this study, which was comparable with the reported values of other membranes, e.g., Hb/ZrO_2/chitosan (1.8 mM),[45] Hb/ZrO_2 (1.6 mM),[46] and Hb/SP Sephadex (1.9 mM).[47]

3.4. Reproducibility and Stability of PS-*b*-PAA/Hb Electrode. Both reproducibility and stability are key criteria of an electrode for a practical application. Six PS-*b*-PAA/Hb electrodes were individually fabricated and tested with 1 mM of H_2O_2 at −0.25 V vs SCE. The relative standard deviation of the current response was 5.54%, which included errors from both the fabrication and the measurement. The operating stability of the PS-*b*-PAA/Hb electrode was evaluated by CV (see Figure S1 in the Supporting Information). The peak potential barely changed, and the peak current after 50 cycles remained 96.5% of the one in the first cycle. The time stability was evaluated at −0.25 V vs SCE. The PS-*b*-PAA/Hb electrode was stored at 4 °C and the current response to 1 mM of H_2O_2 was measured after every several days. The electrode was found to be able to retain 85% of its current after 30 days (see Figure S2 in the Supporting Information). The good stability of the PS-*b*-PAA/Hb electrode could be ascribed to the strong and favorable electrostatic interaction between Hb and the PAA block.

4. CONCLUSION

In this study, a facile method was developed to fabricate an Hb-immobilized polymeric membrane on a GCE substrate via solution casting and evaporation coupled with the CADD self-assembly. The self-assembly of Hb and PS-*b*-PAA brought the membrane hydrophobic and porous surface. The electrostatic interaction together with the hydrophilicity of Hb and the PAA block led them to be detained in the lower layer of water. The hydrophobic PS chain rather stayed in the upper layer of $CHCl_3$ to form a hydrophobic surface after drying. The electrochemical reaction on this PS-*b*-PAA/Hb electrode exhibited a surface-controlled electrode process. The immobilized Hb retained its native biological activity and high catalytic ability to H_2O_2. The electrode showed a good reproducibility, operating stability and time stability. The sensitivity of the electrode was determined to be 4.0 mA·M^{-1}·cm^{-2} with a linear range from 2.0×10^{-5} to 1.0×10^{-3} M. The detection limit was estimated to be 1.2×10^{-5} M. This facile CADD self-assembly technique with a polyelectrolyte-based amphiphilic diblock copolymer might have potential use for constructing a third generation biosensor.

DOI: 10.1021/acsami.5b01487
ACS Appl. Mater. Interfaces 2015, 7, 8852–8858

■ ASSOCIATED CONTENT

Supporting Information

The operating and time stability of the electrode. This material is available free of charge via the Internet at http://pubs.acs.org.

■ AUTHOR INFORMATION

Corresponding Author

*E-mail: chhgxue@yzu.edu.cn. Tel.: +86-514-87975436. Fax: +86-514-87975244.

Notes

The authors declare no competing financial interest.

■ ACKNOWLEDGMENTS

The authors are grateful to the financial supports from the National Natural Science Foundation of China (Grant 21173183), 333 Project of Jiangsu Province (Grant BRA2011188), Jiangsu Provincial Plans of Research and Innovation for Graduate Students (Grant CXZZ120895), and the Priority Academic Program Development of Jiangsu Higher Education Institutions. Zhengxi Zhu thanks the financial support from Lvyangjinfeng talent program of Yangzhou.

■ REFERENCES

(1) Fenzl, C.; Hirsch, T.; Wolfbeis, O. S. Photonic Crystals for Chemical Sensing and Biosensing. *Angew. Chem., Int. Ed.* **2014**, *53*, 3318−3335.

(2) Ding, C.; Zhu, A.; Tian, Y. Functional Surface Engineering of C-Dots for Fluorescent Biosensing and in Vivo Bioimaging. *Acc. Chem. Res.* **2014**, *47*, 20−30.

(3) van Grinsven, B.; Eersels, K.; Peeters, M.; Losada-Perez, P.; Vandenryt, T.; Cleij, T. J.; Wagner, P. The Heat-Transfer Method: A Versatile Low-Cost, Label-Free, Fast, and User-Friendly Readout Platform for Biosensor Applications. *ACS Appl. Mater. Interfaces* **2014**, *6*, 13309−13318.

(4) Park, B.-W.; Yoon, D.-Y.; Kim, D.-S. Recent Progress in Bio-Sensing Techniques with Encapsulated Enzymes. *Biosens. Bioelectron.* **2010**, *26*, 1−10.

(5) Samanta, D.; Sarkar, A. Immobilization of Bio-Macromolecules on Self-Assembled Monolayers: Methods and Sensor Applications. *Chem. Soc. Rev.* **2011**, *40*, 2567−2592.

(6) Hartmann, M.; Kostrov, X. Immobilization of Enzymes on Porous Silicas - Benefits and Challenges. *Chem. Soc. Rev.* **2013**, *42*, 6277−6289.

(7) Sassolas, A.; Blum, L. J.; Leca-Bouvier, B. D. Immobilization Strategies to Develop Enzymatic Biosensors. *Biotechnol. Adv.* **2012**, *30*, 489−511.

(8) Huang, Y.; Wang, W.; Li, Z.; Qin, X.; Bu, L.; Tang, Z.; Fu, Y.; Ma, M.; Xie, Q.; Yao, S.; Hu, J. Horseradish Peroxidase-Catalyzed Synthesis of Poly(thiophene-3-boronic acid) Biocomposites for Mono-/Bi-Enzyme Immobilization and Amperometric Biosensing. *Biosens. Bioelectron.* **2013**, *44*, 41−47.

(9) Shim, J.; Kim, G.-Y.; Moon, S.-H. Covalent co-Immobilization of Glucose Oxidase and Ferrocenedicarboxylic Acid for an Enzymatic Biofuel Cell. *J. Electroanal. Chem.* **2011**, *653*, 14−20.

(10) Gupta, R.; Chaudhury, N. K. Entrapment of Biomolecules in Sol-Gel Matrix for Applications in Biosensors: Problems and Future Prospects. *Biosens. Bioelectron.* **2007**, *22*, 2387−2399.

(11) Fan, Q.; Shan, D.; Xue, H. G.; He, Y.; Cosnier, S. Amperometric Phenol Biosensor Based on Laponite Clay-Chitosan Nanocomposite Matrix. *Biosens. Bioelectron.* **2007**, *22*, 816−821.

(12) Yang, G.; Kampstra, K. L.; Abidian, M. R. High-Performance Conducting Polymer Nanofiber Biosensors for Detection of Biomolecules. *Adv. Mater.* **2014**, *26*, 4954−4960.

(13) Cosnier, S.; Holzinger, M. Electrosynthesized Polymers for Biosensing. *Chem. Soc. Rev.* **2011**, *40*, 2146−2156.

(14) Iost, R. M.; Crespilho, F. N. Layer-by-Layer Self-Assembly and Electrochemistry: Applications in Biosensing and Bioelectronics. *Biosens. Bioelectron.* **2012**, *31*, 1−10.

(15) Luo, W.; Li, Y.; Dong, J.; Wei, J.; Xu, J.; Deng, Y.; Zhao, D. A Resol-Assisted co-Assembly Approach to Crystalline Mesoporous Niobia Spheres for Electrochemical Biosensing. *Angew. Chem., Int. Ed.* **2013**, *52*, 10505−10510.

(16) Shan, D.; Han, E.; Xue, H. G.; Cosnier, S. Self-Assembled Films of Hemoglobin/Laponite/Chitosan: Application for the Direct Electrochemistry and Catalysis to Hydrogen Peroxide. *Biomacromolecules* **2007**, *8*, 3041−3046.

(17) Shan, D.; Wang, S.; Xue, H. G.; Cosnier, S. Direct Electrochemistry and Electrocatalysis of Hemoglobin Entrapped in Composite Matrix Based on Chitosan and $CaCO_3$ Nanoparticles. *Electrochem. Commun.* **2007**, *9*, 529−534.

(18) Xia, L.; Wei, Z.; Wan, M. Conducting Polymer Nanostructures and Their Application in Biosensors. *J. Colloid Interface Sci.* **2010**, *341*, 1−11.

(19) Hasanzadeh, M.; Shadjou, N.; de la Guardia, M. Electrochemical Biosensing Using Hydrogel Nanoparticles. *Trends Anal. Chem.* **2014**, *62*, 11−19.

(20) Mousty, C. Biosensing Applications of Clay-Modified Electrodes: A Review. *Anal. Bioanal. Chem.* **2010**, *396*, 315−325.

(21) Teles, F. R. R.; Fonseca, L. R. Applications of Polymers for Biomolecule Immobilization in Electrochemical Biosensors. *Mater. Sci. Eng., C* **2008**, *28*, 1530−1543.

(22) Dey, P.; Adamovski, M.; Friebe, S.; Badalyan, A.; Mutihac, R.-C.; Paulus, F.; Leimkuehler, S.; Wollenberger, U.; Haag, R. Dendritic Polyglycerol-Poly(ethylene glycol)-Based Polymer Networks for Biosensing Application. *ACS Appl. Mater. Interfaces* **2014**, *6*, 8937−8941.

(23) Schyrr, B.; Pasche, S.; Voirin, G.; Weder, C.; Simon, Y. C.; Foster, E. J. Biosensors Based on Porous Cellulose Nanocrystal-Poly(vinyl alcohol) Scaffolds. *ACS Appl. Mater. Interfaces* **2014**, *6*, 12674−12683.

(24) Maruyama, N.; Koito, T.; Nishida, J.; Sawadaishi, T.; Cieren, X.; Ijiro, K.; Karthaus, O.; Shimomura, M. Mesoscopic Patterns of Molecular Aggregates on Solid Substrates. *Thin Solid Films* **1998**, *327−329*, 854−856.

(25) Yabu, H.; Shimomura, M. Single-Step Fabrication of Transparent Superhydrophobic Porous Polymer Films. *Chem. Mater.* **2005**, *17*, 5231−5234.

(26) Widawski, G.; Rawiso, M.; Francois, B. Self-Organized Honeycomb Morphology of Star-Polymer Polystyrene Films. *Nature* **1994**, *369*, 387−389.

(27) Francois, B.; Pitois, O.; Francois, J. Polymer Films with a Self-Organized Honeycomb Morphology. *Adv. Mater.* **1995**, *7*, 1041−1044.

(28) Govor, L. V.; Bashmakov, I. A.; Kiebooms, R.; Dyakonov, V.; Parisi, J. Self-Organized Networks Based on Conjugated Polymers. *Adv. Mater.* **2001**, *13*, 588−591.

(29) Karthaus, O.; Maruyama, N.; Cieren, X.; Shimomura, M.; Hasegawa, H.; Hashimoto, T. Water-Assisted Formation of Micrometer-Size Honeycomb Patterns of Polymers. *Langmuir* **2000**, *16*, 6071−6076.

(30) Perutz, M. F.; Wilkinson, A. J.; Paoli, M.; Dodson, G. G. The Stereochemical Mechanism of the Cooperative Effects in Hemoglobin Revisited. *Annu. Rev. Biophys. Biomol. Struct.* **1998**, *27*, 1−34.

(31) Peng, J.; Xuan, Y.; Wang, H. F.; Yang, Y. M.; Li, B. Y.; Han, Y. C. Solvent-Induced Microphase Separation in Diblock Copolymer Thin Films with Reversibly Switchable Morphology. *J. Chem. Phys.* **2004**, *120*, 11163−11170.

(32) Yu, B.; Sun, P.; Chen, T.; Jin, Q.; Ding, D.; Li, B.; Shi, A. C. Self-Assembled Morphologies of Diblock Copolymers Confined in Nanochannels: Effects of Confinement Geometry. *J. Chem. Phys.* **2007**, *126*, 2049031−2049035.

(33) Matsuda, H.; Ayabe, Y. Zur Theorie Der Randles-Sevcikschen Kathodenstrahl-Polarographie. *Z. Elektrochem.* **1955**, *59*, 494−499.

DOI: 10.1021/acsami.5b01487
ACS Appl. Mater. Interfaces 2015, 7, 8852−8858

(34) Sun, W.; Jiang, H.; Jiao, K. Electrochemical Determination of Hydrogen Peroxide Using O-Dianisidine as Substrate and Hemoglobin as Catalyst. *Z. Naturforsch., B: J. Chem. Sci.* **2005**, *117*, 317−322.
(35) Ma, G. X.; Wang, Y. G.; Wang, C. X.; Lu, T. H.; Xia, Y. Y. Hemoglobin Immobilized on Whisker-Like Carbon Composites and its Direct Electrochemistry. *Electrochim. Acta* **2008**, *53*, 4748−4753.
(36) Shan, D.; Cheng, G. X.; Zhu, D. B.; Xue, H. G.; Cosnier, S.; Ding, S. N. Direct Electrochemistry of Hemoglobin in Poly-(acrylonitrile-co-acrylic acid) and its Catalysis to H_2O_2. *Sens. Actuators, B* **2009**, *137*, 259−265.
(37) Shen, L.; Hu, N. F. Heme Protein Films with Polyamidoamine Dendrimer: Direct Electrochemistry and Electrocatalysis. *Biochim. Biophys. Acta, Bioenerg.* **2004**, *1608*, 23−33.
(38) Laviron, E. The Use of Linear Potential Sweep Voltammetry and of A.C. Voltammetry for the Study of the Surface Electrochemical Reaction of Strongly Adsorbed Systems and of Redox Modified Electrodes. *J. Electroanal. Chem. Interfacial Electrochem.* **1979**, *100*, 263−270.
(39) Li, S.; Xia, J.; Liu, C.; Zheng, Y.; Zeng, L.; Hu, J.; Li, Q. Direct Electrochemistry and Electrocatalysis of Hemoglobin on an Indium Tin Oxide Electrode Modified with Implanted Carboxy Ions. *Microchim. Acta* **2009**, *167*, 41−46.
(40) Zhao, Y. D.; Bi, Y. H.; Zhang, W. D.; Luo, Q. M. The Interface Behavior of Hemoglobin at Carbon Nanotube and the Detection for H_2O_2. *Talanta* **2005**, *65*, 489−494.
(41) Wang, L.; Qi, W.; Su, R. X.; He, Z. M. Facile Method to Synthesize Graphene-Zns Nanocomposites: Preparation and Application in Bioelectrochemistry of Hemoglobin. *J. Solid State Electrochem.* **2013**, *17*, 2595−2602.
(42) Liu, H.; Su, X.; Duan, C. Y.; Dong, X. N.; Zhu, Z. F. A Novel Hydrogen Peroxide Biosensor Based on Immobilized Hemoglobin in 3d Flower-Like MoS_2 Microspheres Structure. *Mater. Lett.* **2014**, *122*, 182−185.
(43) Jian, F. F.; Qiao, Y. B.; Zhuang, R. R. Direct Electrochemistry of Hemoglobin in TATP Film: Application in Biological Sensor. *Sens. Actuators, B* **2007**, *124*, 413−420.
(44) Shan, D.; Wang, S. X.; Xue, H. G.; Cosnier, S. Direct Electrochemistry and Electrocatalysis of Hemoglobin Entrapped in Composite Matrix Based on Chitosan and $CaCO_3$ Nanoparticles. *Electrochem. Commun.* **2007**, *9*, 529−534.
(45) Zhao, G.; Feng, J. J.; Xu, J. J.; Chen, H. Y. Direct Electrochemistry and Electrocatalysis of Heme Proteins Immobilized on Self-Assembled ZrO_2 Film. *Electrochem. Commun.* **2005**, *7*, 724−729.
(46) Xu, J.; Liu, C. H.; Teng, Y. L. Direct Electrochemistry and Electrocatalysis of Hydrogen Peroxide Using Hemoglobin Immobilized in Hollow Zirconium Dioxide Spheres and Sodium Alginate Films. *Microchim. Acta* **2010**, *169*, 181−186.
(47) Fan, C. H.; Wang, H. Y.; Sun, S.; Zhu, D. X.; Wagner, G.; Li, G. X. Electron-Transfer Reactivity and Enzymatic Activity of Hemoglobin in a SP Sephadex Membrane. *Anal. Chem.* **2001**, *73*, 2850−2854.

DOI: 10.1021/acsami.5b01487
ACS Appl. Mater. Interfaces 2015, 7, 8852−8858